Supplementary Information for

Magnetic field filtering of the hinge supercurrent in unconventional metal $NiTe_2$-based Josephson junctions

Tian Le[1#], Ruihan Zhang[1,2#], Changcun Li[3], Ruiyang Jiang[1,2], Haohao Sheng[1,2], Linfeng Tu[1,4], Xuewei Cao[4], Zhaozheng Lyu[1,5], Jie Shen[1,6], Guangtong Liu[1,5,6], Fucai Liu[3,7*], Zhijun Wang[1,2*], Li Lu[1,2,5,6*], Fanming Qu[1,2,5,6*]

[1] Beijing National Laboratory for Condensed Matter Physics, Institute of Physics, Chinese Academy of Sciences, Beijing 100190, China

[2] School of Physical Sciences, University of Chinese Academy of Sciences, Beijing 100049, China

[3] School of Optoelectronic Science and Engineering, University of Electronic Science and Technology of China, Chengdu 611731, China

[4] School of Physics, Nankai University, Tianjin 300071, China

[5] Hefei National Laboratory, Hefei 230088, China

[6] Songshan Lake Materials Laboratory, Dongguan, Guangdong 523808, China

[7] Yangtze Delta Region Institute (Huzhou), University of Electronic Science and Technology of China, Huzhou 313009, China

[#] These authors contributed equally to this work.

[*] Emails: fucailiu@uestc.edu.cn; wzj@iphy.ac.cn; lilu@iphy.ac.cn; fanmingqu@iphy.ac.cn

Content

Section I. Extraction of the supercurrent density profile.

In this section, we will introduce the Dynes-Fulton approach for converting the superconducting interference pattern (SIP) $I_c(B_z)$ to the supercurrent density profile $J_s(y)$, taking Figs. 2a and 2b in the main text as an example.

In our configurations, the supercurrent density varies along the y direction. The separation of the two electrodes is L and the width of each electrode is t. Considering the magnetic flux focusing effect of the superconducting electrodes, the effective length of the junction is $L_{eff} = L+t$. The critical supercurrent $I_c(B_z)$ is extracted following the whitish envelope in Fig. 2a which was replotted as Fig. S1a. The red curve in Fig. S1a illustrates $I_c(B_z)$. The experimentally observed $I_c(B_z)$ is the magnitude of the integration of $J_s(y)$. Assuming the normalized magnetic field unit of $\kappa = 2\pi L_{eff} B_z/\Phi_0$, where $\Phi_0 = h/2e$ is the flux quantum (h is the Planck constant and e is the elementary charge), $I_c(B_z)$ can be replaced by the complex critical supercurrent function $\mathfrak{I}_c(\kappa)$:

$$I_c(\kappa) = |\mathfrak{I}_c(\kappa)| = \left|\int_{-\infty}^{\infty} J_s(x) e^{i\kappa y} dy\right|.$$

Considering an even supercurrent density $J_{even}(y)$ with a symmetric distribution, the odd part of $e^{i\kappa y}$ vanishes from the integral, and we can obtain

$$\mathfrak{I}_c(\kappa) = I_{even}(\kappa) = \int_{-\infty}^{\infty} J_{even}(y) \cos(\kappa y) dy.$$

$\mathfrak{I}_c(\kappa)$ in the above formula alternates between positive and negative values at each zero-crossing. Because $I_{even}(\kappa)$ usually dominates in the observed critical supercurrent except at its minima, it can be roughly obtained by multiplying $I_c(\kappa)$ with a flipping function as shown in Fig. S1b, where the sign is switched between adjacent lobes of the whitish envelope. When $I_{even}(\kappa)$ is minimal, $I_c(\kappa)$ is dominated by the odd component: $I_{odd}(\kappa) = \int_{-\infty}^{+\infty} J_{odd}(y)\sin(\kappa y)dy$. $I_{odd}(\kappa)$ can then be approximated by interpolating between the minima of $I_c(\kappa)$, and flipping sign between lobes as shown in Fig. S1c. A Fourier transform of the complex critical supercurrent function $\mathfrak{I}_c(\kappa) = I_{even}(\kappa) + iI_{odd}(\kappa)$ is:

$$J_S(y) = \left|\frac{1}{2\pi}\int_{-W/2}^{W/2} \mathfrak{I}_c(\kappa)e^{-i\kappa y}d\kappa\right|,$$

which produces the supercurrent density profile as shown in Fig. S1d (the same as Fig. 2b).

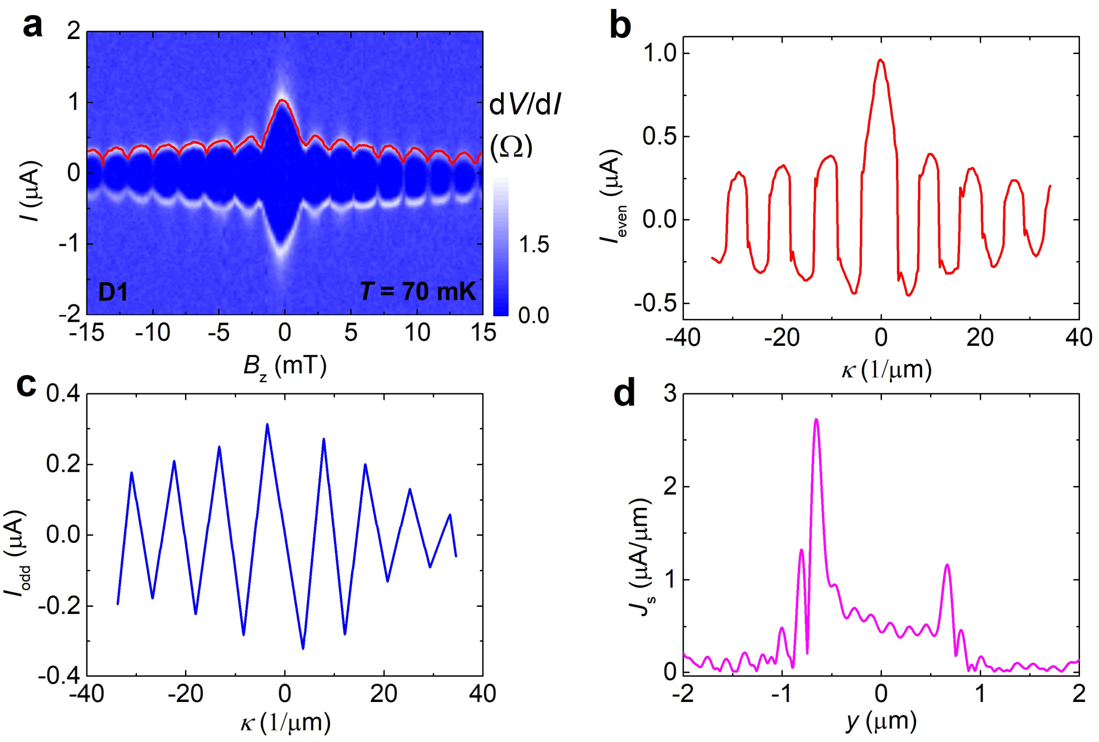

Fig. S1. **a**, SIP for D1, the same as Fig. 2a in the main text. The red curve illustrates $I_c(B_z)$ taken following the whitish envelope for an example. **b**, The even part of $I_c(\kappa)$ recovered from the red curve in **a**. **c**, The odd part of $I_c(\kappa)$ recovered from the red curve in **a**. **d**, Supercurrent density profile for $I_c(B_z)$ in **a**.

Section II. Magnitude of B_x to kill the bulk supercurrent for different devices.

We note that the B_x for killing the bulk supercurrent on D1 is much larger than D2, D3 and D4. We think it is caused by the detailed fabrication process (e.g., the quality of the superconductor films), because D2, D3 and D4 are fabricated simultaneously. However, D1 was fabricated and measured around six months earlier than them. In Fig. S2, we present another device D5, which was fabricated together with D1, and it also shows a larger B_x for killing the bulk supercurrent.

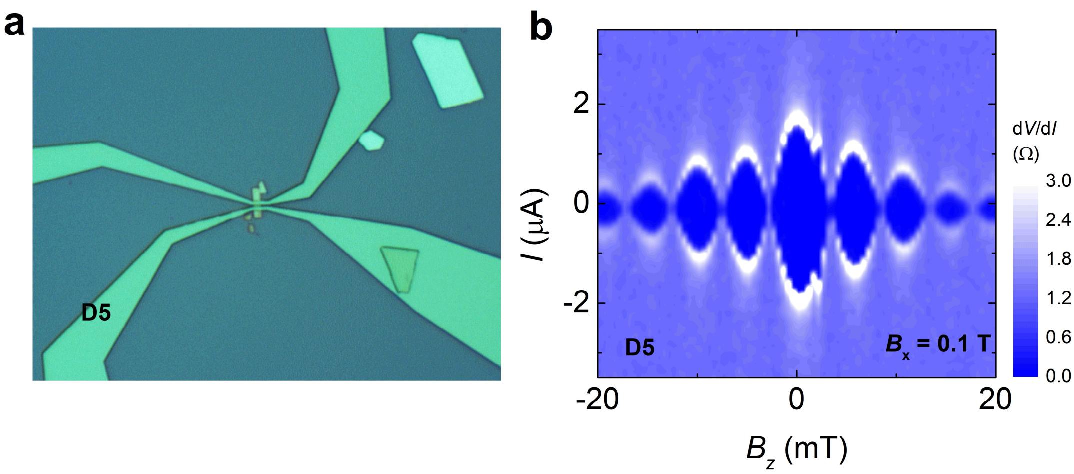

Fig. S2. **a**, The optical image for D5. **b**, SIP for D5 under $B_x = 0.1$ T.

Section III. Anisotropy of bulk supercurrent between B_x and B_y.

As shown by Fig. 4 in the main text, the critical field of bulk supercurrent along B_x is lower than B_y. We think it is a common phenomenon that has been reported on other Josephson junctions with a similar electrode configuration[1]. We attribute it to the vimineous shape of the electrodes that exhibit anisotropic demagnetization N[2]. It is natural to assume the proximity-induced superconducting region beneath the electrodes to be a stripe shape. The effective demagnetization can be approximated as[3]:

$$N^{-1} = 1 + \frac{3}{4}\frac{l_{\parallel}}{l_{\perp}}$$

where the symbol $l_{\parallel}$ represents the length along the magnetic field direction, $l_{\perp}$ is the length perpendicular to the magnetic field. Suppose $l_{\parallel}$ and $l_{\perp}$ are comparable to the size of the electrodes on the sample (2.1 μm × 0.5 μm), and N is estimated to be around 0.84 for B_x and 0.24 for B_y, which produce a large anisotropy.

Section IV. Analysis of the critical side-surface supercurrent (side-surface-I_c) under B_y.

As we mentioned in the main text, if the boundary supercurrent originates from the side surfaces (rather than the hinges), we can calculate its value at a certain B_y through the Fraunhofer-like decay curve. To do so, we need to supress the contribution of the bulk supercurrent, which can be achieved by applying a small B_z to render the Fraunhofer-like $1/|B_z|$ decay of the bulk supercurrent itself. Therefore, we inspect the side lobes of SIP in Fig. 2a in the main text, where the bulk supercurrent has been supressed due to the Fraunhofer diffraction in B_z. Of course, the larger the serial number $|n|$ of the side lobes, the heavier the suppression of the bulk supercurrent. Nevertheless, we assign the height of the side lobes (excluding the central lobe) of the SIP at B_y = 0 T in Fig. 2a as the critical supercurrent of the side-surface, side-surface-I_c. In the main text, we assume that the effective junction length of the side surface is comparable to the separation of the electrodes, i.e., ~300 nm. In fact, it could be underestimated if considering the flux focusing effect of the electrodes. We thus test several conditions here, as shown in Fig. S3, and side-surface-I_c is always smaller than the height of the first lobe ~$0.21I_c^0$, where I_c^0 is the side-surface-I_c at B_y = 0 T. However, the experimental boundary-I_c at B_y = 0.2 T is much larger than $0.21I_c^0$ as shown in Fig. 5c in the main text, in contrast to the side-surface scenario.

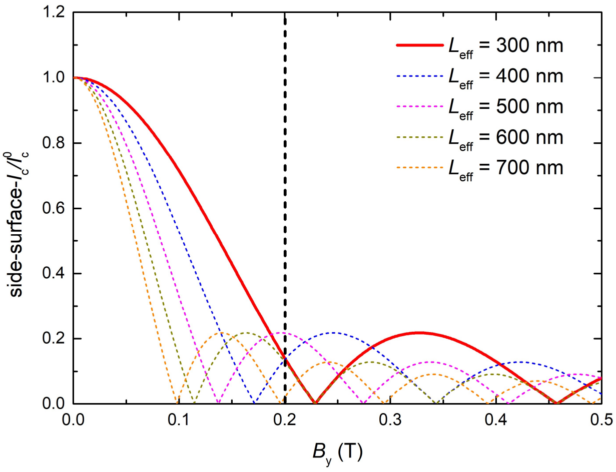

Fig. S3. Simulation of Fraunhofer-like curves for different effective junction lengths assuming a side-surface supercurrent.

Section V. SIP for D1.

Figure S4 shows the SIP for D1 at $B_y = 0.2$ T, which was used to extract the boundary-I_c at $B_y = 0.2$ T for the side lobes presented in Fig. 5c in the main text.

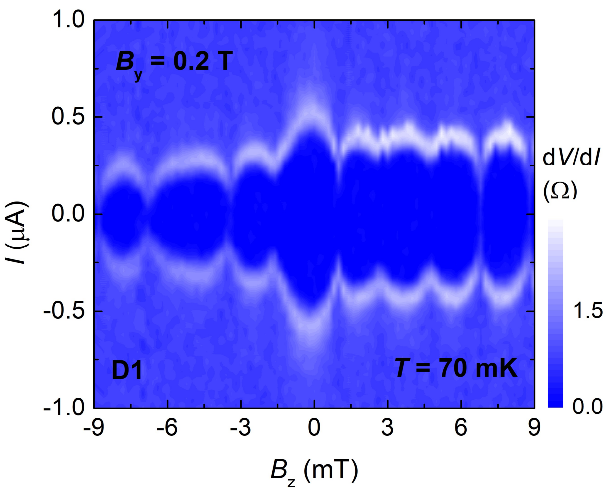

Fig. S4. SIP for D1 at $B_y = 0.2$ T.

Section VI. Theoretical calculation.

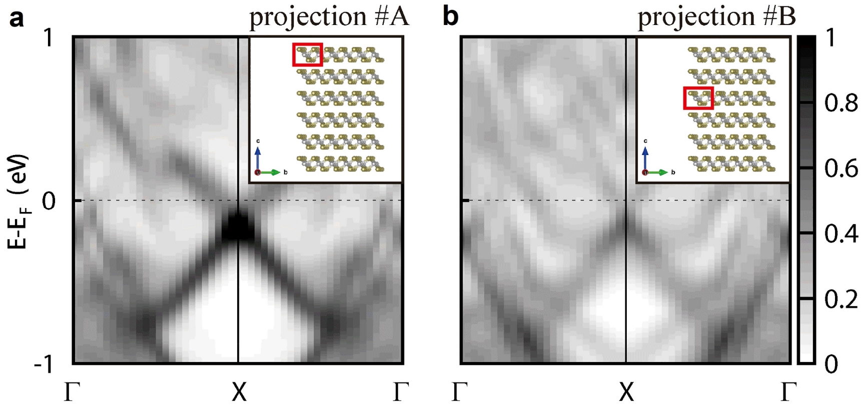

Fig. S5. The bands of **a**, hinge state and **b**, side-surface state. Compared with the side-surface atoms' projection (projection #B), the hinge atoms' projection (projection #A) contributes more around E_F, which indicates that the band contribution near the Fermi level is dominated by the hinge state rather than side-surface state.

1 Baumgartner, C. *et al.* Supercurrent rectification and magnetochiral effects in symmetric Josephson junctions. *Nat. Nano.* **17**, 39-44, (2022).

2 Mi, X. *et al.* Relevance of sample geometry on the in-plane anisotropy of $Sr_xBi_2Se_3$ superconductor. *arXiv: 2110.14447*, (2021).

3 Prozorov, R. & Kogan, V. G. Effective demagnetizing factors of diamagnetic samples of various shapes. *Phys. Rev. Appl.* **10**, 014030, (2018).